p38 signaling inhibits mTORC1-independent autophagy in senescent human CD8$^+$ T cells

Sian M. Henson,[1] Alessio Lanna,[1] Natalie E. Riddell,[1] Ornella Franzese,[2] Richard Macaulay,[1] Stephen J. Griffiths,[1] Daniel J. Puleston,[3] Alexander Scarth Watson,[3] Anna Katharina Simon,[3] Sharon A. Tooze,[4] and Arne N. Akbar[1]

[1]Division of Infection and Immunity, University College London, London, United Kingdom. [2]Department of Systems Medicine, University of Tor Vergata, Rome, Italy. [3]MRC Human Immunology Unit, Weatherall Institute of Molecular Medicine, University of Oxford, Oxford, United Kingdom. [4]Secretory Pathways Laboratory, London Research Institute, Cancer Research UK, London, United Kingdom.

T cell senescence is thought to contribute to immune function decline, but the pathways that mediate senescence in these cells are not clear. Here, we evaluated T cell populations from healthy volunteers and determined that human CD8$^+$ effector memory T cells that reexpress the naive T cell marker CD45RA have many characteristics of cellular senescence, including decreased proliferation, defective mitochondrial function, and elevated levels of both ROS and p38 MAPK. Despite their apparent senescent state, we determined that these cells secreted high levels of both TNF-α and IFN-γ and showed potent cytotoxic activity. We found that the senescent CD45RA-expressing population engaged anaerobic glycolysis to generate energy for effector functions. Furthermore, inhibition of p38 MAPK signaling in senescent CD8$^+$ T cells increased their proliferation, telomerase activity, mitochondrial biogenesis, and fitness; however, the extra energy required for these processes did not arise from increased glucose uptake or oxidative phosphorylation. Instead, p38 MAPK blockade in these senescent cells induced an increase in autophagy through enhanced interactions between p38 interacting protein (p38IP) and autophagy protein 9 (ATG9) in an mTOR-independent manner. Together, our findings describe fundamental metabolic requirements of senescent primary human CD8$^+$ T cells and demonstrate that p38 MAPK blockade reverses senescence via an mTOR-independent pathway.

Introduction

Cellular senescence has predominantly been characterized using fibroblast models, where it is defined as the irreversible loss of proliferative capacity despite continued viability and metabolic activity (1). This arrested cell division arises as a consequence of either telomere-dependent or telomere-independent pathways, the latter being induced as a result of DNA damage by reactive oxygen species (ROS) or the activation of cellular stress pathways (1, 2). Another defining feature of fibroblast senescence is the acquisition of a senescence-associated secretory phenotype (SASP), featuring the secretion of growth factors, proteases, and inflammatory cytokines that affect neighboring cells in a paracrine manner (3). Therefore, senescent cells still have to fulfill the energy requirements for these functions.

It is not clear exactly how senescence manifests itself in T lymphocytes. Like fibroblasts, these cells are highly proliferative, and in response to repeated stimulation, they also experience growth arrest (4–6). It has been proposed that senescent human T cells lose expression of the costimulatory receptor CD28, exhibit increased expression of surface KLRG1 and/ or CD57, have short telomeres associated with low telomerase activity, and show a decreased capacity for expansion after activation (7–9). Functional data examining the mechanisms of senescence have predominately used the loss of CD28 expression to define senescent T cells; however, the CD28$^-$ population is very heterogeneous and encompasses both effector and senescent cells (10, 11). However, more definitive characteristics of senescence, including markers of the DNA damage response and p38 MAPK activation, have not been investigated in parallel with KLRG1 and CD57. The first aim of the present study was to combine multiple markers of senescence to characterize which primary human CD8$^+$ T cells have characteristics of senescence.

In rodents, effector T cells preferentially engage glycolysis over oxidative phosphorylation (OXPHOS) to generate the energy required for functional activity, despite the fact that the former process is much less efficient at generating ATP from glucose (12). However, it is not known how senescent human CD8$^+$ T cells generate the energy required for their functional activity. Furthermore, previous studies have shown that blocking p38 signaling can reverse some senescence-associated defects in human T cells, such as low proliferation and telomerase activity after stimulation (13). However, it is not known how the extra energy required for these functions is generated. p38 is activated both by environmental stressors, such as DNA damage, and by ROS and proinflammatory cytokines, via a canonical signaling pathway involving a kinase activation cascade that culminates in the phosphorylation of p38 MAPK (14). In T cells, there is an alternative pathway that directly couples TCR ligation to p38 activation, allowing T cells to activate p38 under nonstressful conditions (15). p38 also plays an important role in senescence growth arrest due to its ability to activate both the p53 and pRb/p16 growth arrest pathways (16); however, its role in regulating T cell metabolism is not known.

In the present study, we found that effector memory CD8$^+$ T cells that reexpress CD45RA (EMRA) exhibited multiple charac-

Conflict of interest: The authors have declared that no conflict of interest exists.
Submitted: January 6, 2014; **Accepted:** June 13, 2014.
Reference information: *J Clin Invest*. doi:10.1172/JCI75051.

teristics of senescence, yet had potent functional activity, including cytotoxic activity and secretion of TNF-α and IFN-γ after activation. However, these cells had very low proliferative activity. In contrast, the effector memory (EM) CD8$^+$ T cell population was also functionally potent, but also highly proliferative compared with the senescent CD8$^+$ T cells. We found that while EM CD8$^+$ T cells used OXPHOS in conjunction with glycolysis to generate energy, the senescent EMRA CD8$^+$ T cells used anaerobic glycolysis preferentially. Senescent CD8$^+$ T cells produced more ROS and exhibited mitochondrial dysfunction, which may explain their dependence on glycolysis for energy. A key observation was that p38 signaling in these cells increased mitochondrial biogenesis as well as telomerase and proliferative activity after activation. The senescent CD8$^+$ T cells also retained most of their effector functions after p38 blockade, which suggests that these cells require more energy than unblocked cells. We found that despite their reversal of mitochondrial defects, these cells still preferentially engaged anaerobic glycolysis after p38 inhibition. Furthermore, the additional energy required for proliferation was obtained from autophagy, via an mTOR-independent pathway. We therefore concluded that the extra energy required for the reconstituted proliferative activity in senescent CD8$^+$ T cells after p38 blockade is generated by the recycling of intracellular macromolecules.

Results

EMRA CD8$^+$ T cells exhibit phenotypic, functional, and DNA damage response parameters characteristic of senescence. Human CD8$^+$ T cells can be subdivided into 4 populations on the basis of their relative surface expression of CD45RA and CD27 molecules (Supplemental Figure 1A; supplemental material available online with this article; doi:10.1172/JCI75051DS1). These subsets — naive (CD45RA$^+$CD27$^+$), central memory (CM; CD45RA$^-$CD27$^+$), EM (CD45RA$^-$CD27$^-$), and EMRA (CD45RA$^+$CD27$^-$) — are analogous to those identified in other reports in which surface CCR7 together with CD45RA expression were used to distinguish among T cells at different stages of differentiation (17). In previous studies, based on cell surface phenotype alone, the EMRA subset has been postulated to represent a senescent population of cells that accumulated with age and certain diseases (18). In the present study, EMRA CD8$^+$ T cells were found to constitute between 4% and 42% of the CD8$^+$ compartment (median, 22%). The first aim of this study was to provide an unequivocal definition of a senescent human CD8$^+$ T cell population by investigating multiple phenotypic and functional parameters of senescence.

We investigated the surface coexpression of KLRG1 and CD57, which have been proposed to identify senescent T cells (7, 9), as well as phosphorylated H2AX (γH2AX), a member of the histone H2A family that is part of the DNA damage response (DDR) in senescent cells (19) isolated from young individuals. Although senescent cells accumulate during aging (20), some are also found in young subjects as a result of antigenic stimulation (21). We found that after stimulation, the EMRA CD8$^+$ T cells expressed the greatest number of senescence markers simultaneously (Figure 1A). However, not all EMRA CD8$^+$ T cells were senescent; 30% of this population displayed no markers of senescence. In addition, it has previously been shown that memory T cells have significantly shorter telomeres than the naive population (13, 22), which indicates that they have experienced more cycles of proliferation. We found that the EMRA CD8$^+$ T cells had the lowest telomerase activity after activation (Figure 1B).

p38 MAPK is activated in response to DNA damage and plays a central role in inducing senescence due to its ability to activate both p53 and pRb/p16 pathways (16, 23). The high expression levels of phosphorylated p38 (p-p38) MAPK were detected in the EMRA subset after stimulation, as determined by Western blot and flow cytometric analysis (Figure 1, C and D). ROS can induce DNA damage and senescence by activating p53 (2). We found that production of both mitochondrial and cytoplasmic ROS (measured by MitoSOX and DHE, respectively) were significantly higher in EMRA CD8$^+$ T cells compared with all other subsets (Figure 1, E and F, and Supplemental Figure 1B).

The key attribute and defining feature of senescence is growth arrest, and we found that EMRA CD8$^+$ T cells showed significantly less proliferative activity after activation than the other subsets (Figure 1G). Despite this, these cells had potent effector activity — as shown by their greater polyfunctionality, measured by flow cytometry (TNF-α, IFN-γ, perforin, and granzyme per cell) — compared with the other subsets (Figure 1H). Therefore, EMRA CD8$^+$ T cells have multiple phenotypic and functional characteristics of cellular senescence, including low proliferative activity, but have the characteristics of potent effector T cells.

EMRA CD8$^+$ T cells exhibit mitochondrial impairment. The increased level of ROS in the senescent CD8$^+$ T cell population raised the possibility that there were alterations in mitochondrial function in these cells. We therefore examined the mitochondria in the CD8$^+$ T cell subsets, stimulated overnight with anti-CD3 and IL-2, by electron microscopy (Figure 2A). We observed significantly fewer mitochondria in EMRA CD8$^+$ T cells compared with the other memory subsets using a point counting method to quantitate these organelles (Figure 2B). We also stained stimulated CD8$^+$ T cells with MitoTracker Green, a mitochondrial-specific dye that binds the mitochondrial membranes independently of mitochondrial membrane potential (MMP), which has been used as a quantitative assessment of mitochondrial mass (24). Mitochondrial mass was highest in CM and EM CD8$^+$ T cells, and the EMRA subset displayed a significantly lower mitochondrial mass than EM CD8$^+$ T cells (Figure 2, C and D). We further confirmed the lower mitochondrial content in EMRA CD8$^+$ T cells by examining the ratio of mitochondrial DNA to nuclear DNA (mtDNA/nDNA), which also confirmed that EMRA CD8$^+$ T cells displayed significantly less mitochondrial mass than the CM and EM subsets ($P < 0.05$; Figure 2E). The lower mitochondrial content in the activated EMRA CD8$^+$ T cells was not due to the unresponsiveness of these cells, as no significant difference in expression of the activation marker CD69 was found among all 4 subsets after stimulation (Supplemental Figure 2, A–C).

We next investigated mitochondrial function by examining MMP in different subsets in freshly isolated PBMCs, after overnight stimulation with anti-CD3 antibody, using the lipophilic cation JC-1 (Figure 2, F and G). JC-1 is mitochondria selective and forms aggregates in polarized mitochondria that result in a green-orange emission after excitation. However, the monomeric form present in cells with depolarized mitochondrial membranes emits only green fluorescence. We found MMP to be decreased

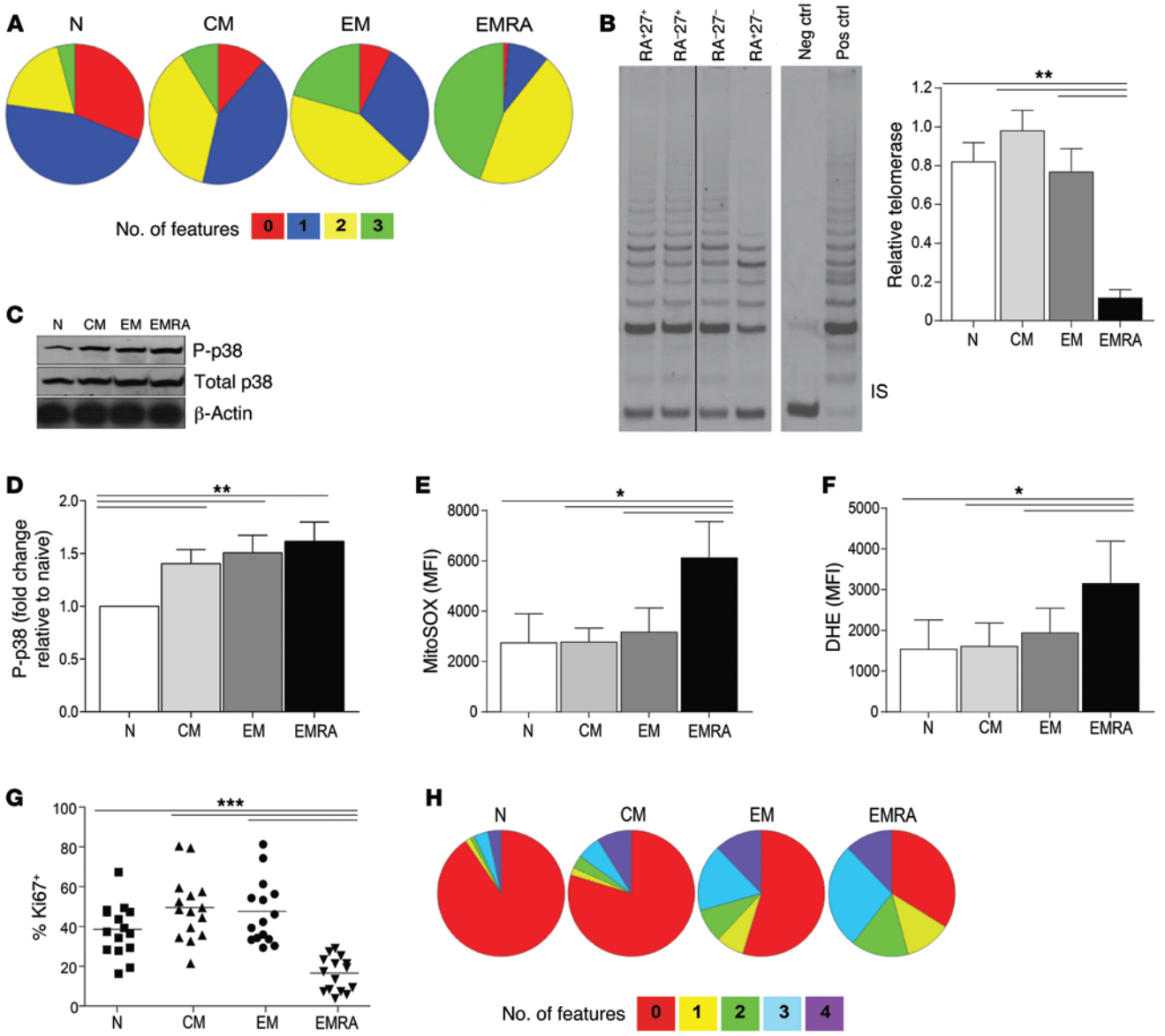

Figure 1. EMRA CD8⁺ T cells exhibit characteristics of senescent T cells. (**A**) Multiparameter flow cytometry examining expression of the senescence features KLRG1, CD57, and γH2AX in the 4 CD45RA/CD27-defined CD8⁺ T cell subsets after an 8-hour stimulation with 0.5 μg/ml anti-CD3. Pie charts show the average of 7 donors. N, naive. (**B**) Representative blot showing telomerase activity on day 3 after activation with 0.5 μg/ml anti-CD3 and 5 ng/ml IL-2 (n = 4). Lanes were run on the same gel but were noncontiguous (black line). Telomerase activity was calculated by densitometry and expressed in arbitrary units relative to the internal standard (IS). (**C**) Representative immunoblots of p-p38 and total p38 together with β-actin after a 30-minute stimulation with 0.5 μg/ml anti-CD3 and 5 ng/ml IL-2. (**D**) Phosphoflow data after a 30-minute stimulation with 0.5 μg/ml PMA and ionomycin. Data are shown relative to the naive subset, n = 9. (**E** and **F**) ROS production, obtained using MitoSox (**E**) and DHE (**F**), in the CD8⁺ T cell subsets after overnight stimulation (n = 8). (**G**) Proliferation of CD8⁺ T cell subsets, assessed by Ki67 staining, after stimulation with 0.5 μg/ml anti-CD3 and 5 ng/ml IL-2 for 3 days. Horizontal lines depict means. (**H**) Multiparameter flow cytometry examining expression of IFN-γ, TNF-α, perforin, and granzyme B after an 8-hour stimulation with 0.5 μg/ml anti-CD3. Pie charts show the average of 7 donors. *P < 0.05, **P < 0.01, ***P < 0.001, repeated-measures ANOVA followed by Tukey correction.

in EMRA CD8⁺ T cells (Figure 2, F and G), indicative of the presence of dysfunctional depolarized mitochondria. Together, these data showed that EMRA CD8⁺ T cells have lower mitochondrial content than other memory subsets and that what mitochondria remain are more dysfunctional.

EMRA CD8⁺ T cells undergo anaerobic glycolysis. Decreased mitochondrial function in aged liver and muscle cells has been shown to result in a decline in energy production, causing metabolic reprogramming toward extramitochondrial energy production (25). We next investigated whether decreased mitochondrial function in EMRA CD8⁺ T cells is associated with differences in their metabolism compared with the other memory subsets. We first investigated whether there were differences in the way that CD8⁺ T cell subsets were able to use exogenous glucose, by assessing their expression of the glucose transporter Glut1 (26). EMRA CD8⁺ T cells showed the lowest expression of this transporter molecule (Figure 3, A and B), which suggests that this subset may not be able to access extracellular glucose as effectively as the other subsets.

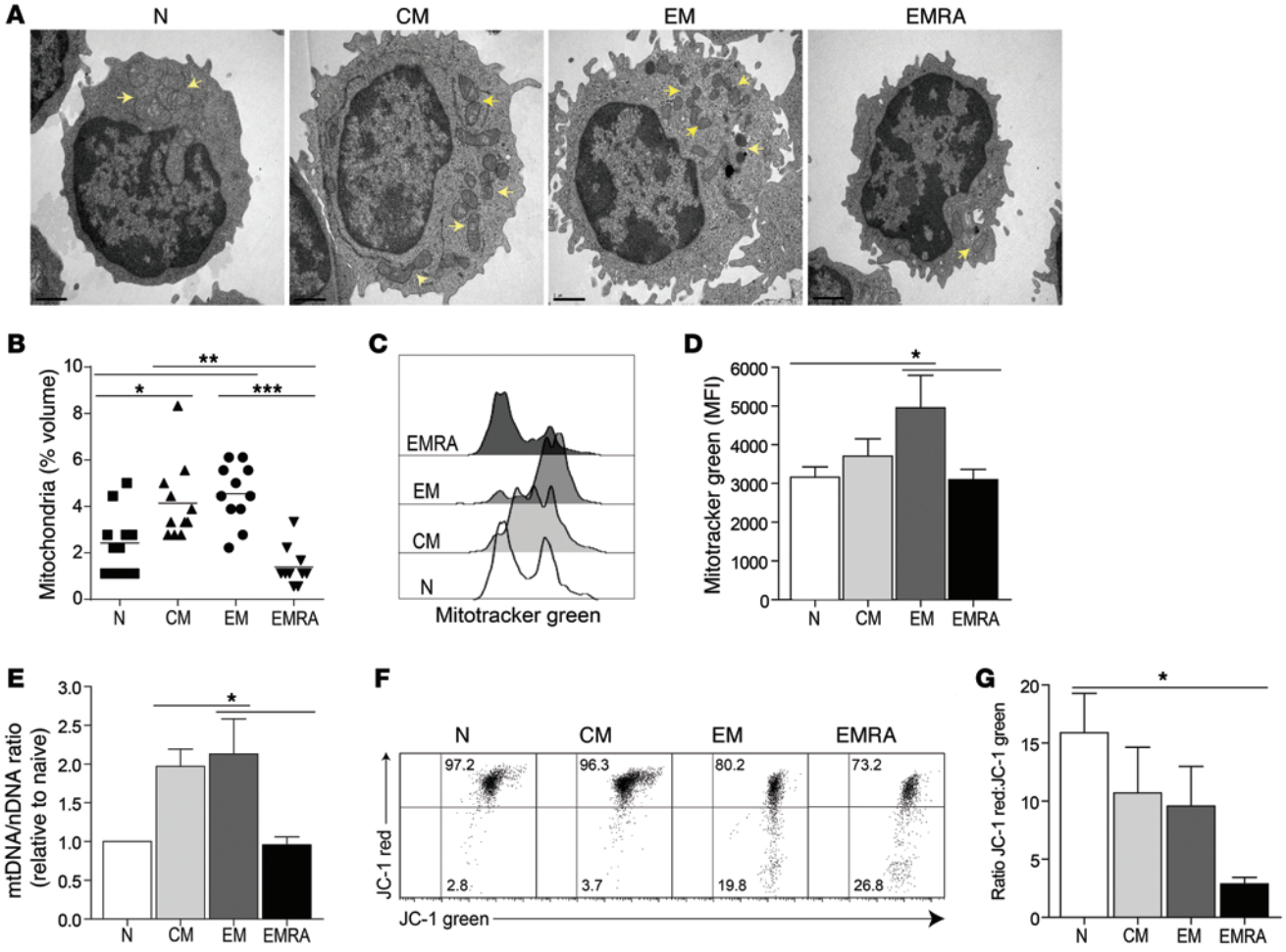

Figure 2. EMRA CD8⁺ T cells display mitochondrial impairment after stimulation. CD45RA/CD27-defined CD8⁺ T cells were stimulated overnight with 0.5 μg/ml anti-CD3 and 5 ng/ml IL-2. (**A**) Electron microscope images. Arrows denote mitochondria. Scale bars: 1 μM. (**B**) Percentage by cell volume of mitochondria, determined by a point counting grid method from 10 different electron microscope images. (**C** and **D**) Representative examples (**C**) and data (**D**) showing the expression of Mitotracker Green (n = 8). (**E**) mtDNA/nDNA ratio (n = 4). (**F** and **G**) Representative example (**F**) and data (**G**) showing JC-1 staining (n = 5). The percentage of cells expressing JC-1 red and/or JC-1 green is indicated within the respective quadrants. *P < 0.05, **P < 0.01, ***P < 0.001, repeated-measures ANOVA followed by Tukey correction.

We next measured the bioenergetic profiles of stimulated CD45RA/CD27-defined CD8⁺ T cell subsets after a mitochondrial stress test (Figure 3C), which includes the addition of pharmacological inhibitors of OXPHOS. 3 different compounds are added in succession, altering the bioenergetic profile of the T cells (27). The first compound is oligomycin, an ATP coupler that inhibits ATP synthesis by blocking complex V and is used to distinguish the percentage of oxygen consumption dedicated to ATP synthesis and to overcome the natural proton leak across the inner mitochondrial membrane. The second is FCCP, which uncouples ATP synthesis from the electron transport chain by transporting H^+ ions across the inner mitochondrial membrane. The collapse of the MMP leads to the consumption of both oxygen and energy without generating ATP and is used to calculate the spare respiratory capacity (SRC). The third is a mixture of rotenone and antimycin A, which blocks complexes I and III, respectively, of the electron transport chain, shutting down mitochondrial respiration and thereby allowing for calculation of both the mitochondrial and nonmitochondrial fractions contributing to respiration (Supplemental Figure 2D).

The key features of note in this mitochondrial stress test were the higher basal metabolic rate and oxygen consumption rate (OCR), together with greater SRC, in the CM and EM subsets compared with the naive and EMRA populations (Figure 3C). This increased OCR was an indicator of CM and EM CD8⁺ T cells undergoing OXPHOS. However, the extracellular acidification rate (ECAR), a marker of lactic acid production and glycolysis, was higher in EM and EMRA CD8⁺ T cells than the naive and CM subsets (Figure 3D). This suggests that naive T cells have low ability to perform OXPHOS and glycolysis and are highly dependent on exogenous glucose to generate energy. Moreover, CM CD8⁺ T cells mainly utilize OXPHOS, whereas the EMRA population mainly utilizes glycolysis, and the EM subset exhibits the greatest metabolic versatility, able to engage either OXPHOS or glycolysis after TCR activation. The EM and EMRA subsets were also found to have the lowest OCR/ECAR ratios (Figure 3E), further strengthening the idea that these cells undergo glycolysis.

SRC, the mitochondrial capacity available to cells in order to produce energy under conditions of increased effort or stress, is

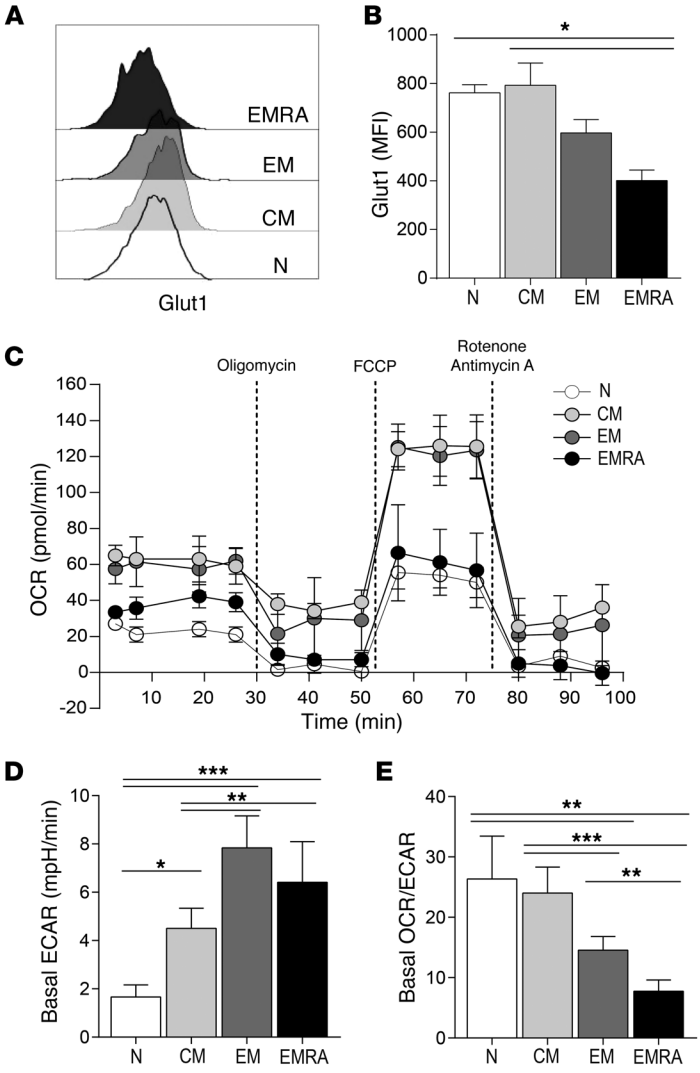

Figure 3. EMRA CD8⁺ T cells undergo anaerobic glycolysis. (**A** and **B**) Examples (**A**) and data (**B**) showing Glut1 expression within CD45RA/CD27-defined CD8⁺ T cell subsets after overnight stimulation with 0.5 μg/ml anti-CD3 (n = 8). (**C**) OCR of CD8⁺ T cell subsets were measured after overnight stimulation with 0.5 μg/ml anti-CD3 and 5 ng/ml IL-2, and cells were then subjected to a metabolic stress test using the indicated mitochondrial inhibitors. Data are representative of 4 independent experiments. (**D** and **E**) Basal ECAR (**D**) and basal OCR/ECAR ratio (**E**) of the CD8⁺ T cell subsets after overnight stimulation with 0.5 μg/ml anti-CD3 and 5 ng/ml IL-2 (n = 4). $^*P < 0.05$, $^{**}P < 0.01$, $^{***}P < 0.001$, repeated-measures ANOVA followed by Tukey correction.

important for long-term survival and function (28). Collectively, the lower SRC in EMRA CD8⁺ T cells together with lower mitochondrial mass (Figure 2, A–E), increased ROS production (Figure 1, E and F), and decreased MMP (Figure 2, F and G) suggests that these cells are very metabolically unstable compared with the other memory subsets, yet are still able to generate sufficient energy for effector functions (Figure 1G).

p38 MAPK inhibition partially restores mitochondrial function in EMRA CD8⁺ T cells. Previous studies in CD4⁺ T cells have shown that the decreased proliferation and telomerase activity in the highly differentiated EMRA subset can be partially restored by blocking p38 MAPK activity with the specific small-molecule inhibitor BIRB 796 (13). When used at a concentration of 500 nM, BIRB 796 specifically inhibits p38 MAPK (13). We therefore investigated whether blocking p38 in EMRA CD8⁺ T cells had the same effect. Addition of BIRB 796 to EMRA CD8⁺ T cells enhanced both their proliferation and their telomerase activity after activation (Figure 4, A–D). Inhibition of p38 signaling significantly reduced TNF-α, but not granzyme B, perforin, or IFN-γ, by EMRA CD8⁺ T cells, as measured by flow cytometry (Figure 4E). This raised the question of whether p38 inhibition would affect mitochondrial function and/or metabolic pathways for energy production in these cells.

Naive, CM, EM, and EMRA CD8⁺ T cells were next stimulated in the presence of BIRB 796 or DMSO control for 3 days, and the effect on mitochondrial mass was investigated. Only the EMRA subset responded to treatment with BIRB 796 (Supplemental Figure 2E). After activation of these cells for 3 days, giant mitochondria lacking cristae were observed in the EMRA population (Figure 5A). Electron microscope images showed that after p38 MAPK blockade, the mitochondrial architecture was restored, and the giant mitochondria were no longer present (Figure 5A). Furthermore, the EMRA CD8⁺ T cells incubated with BIRB 796 contained significantly more mitochondria per unit volume of cytoplasm, which was confirmed by measurement of mitochondrial mass using MitoTracker green (Figure 5, B–D). We then investigated whether the increased mitochondrial mass caused by BIRB 796 was associated with improved function; after stimulation in the presence of BIRB 796, MMP (JC-1 red/JC-1 green ratio) increased significantly in EMRA CD8⁺ T cells (Figure 5, E and F). Therefore, inhibition of p38 signaling in EMRA CD8⁺ T cells caused an increase in the number of mitochondria, which were also more functional. This raises the question of whether this leads to an increase in OXPHOS to support the extra energy required for enhanced proliferative activity in the EMRA population.

We addressed this by performing a mitochondrial stress test on EMRA CD8⁺ T cells after 3 days of stimulation in the presence of BIRB 796. The bioenergetic profile revealed no change in OCR between EMRA CD8⁺ T cells incubated with or without BIRB 796 (Figure 6A). ECAR revealed that EMRA CD8⁺ T cells incubated with BIRB 796 produced more lactic acid (Figure 6B), indicative of increased glycolysis. Taken together with the observed drop in OCR/ECAR ratio (Figure 6C), these results suggest that, despite the enhanced mitochondrial function after p38 MAPK inhibition, EMRA CD8⁺ T cells still engage glycolysis to provide the energy required for the increase in proliferation after activation.

Increased energy demand with p38 inhibition is met by increased autophagy via an mTORC1-independent mechanism. Although EMRA CD8⁺ T cells are dependent on glycolysis, they may not be able to increase their metabolic needs by increasing their uptake of extracellular glucose, since these cells expressed relatively low levels of the glucose transporter Glut1 (Figure 3, A and B), which was not changed after treatment with BIRB 796 (Figure 6D). This raised the question of how these cells fuel the increase in glycolysis. One possible nutrient source when extracellular nutrient uptake is insufficient to meet cellular energy demands is macroautophagy (autophagy). We therefore used an imaging flow cytometry–based assay (ImageStream) to assess autophagy in all 4 CD8⁺ T cell sub-

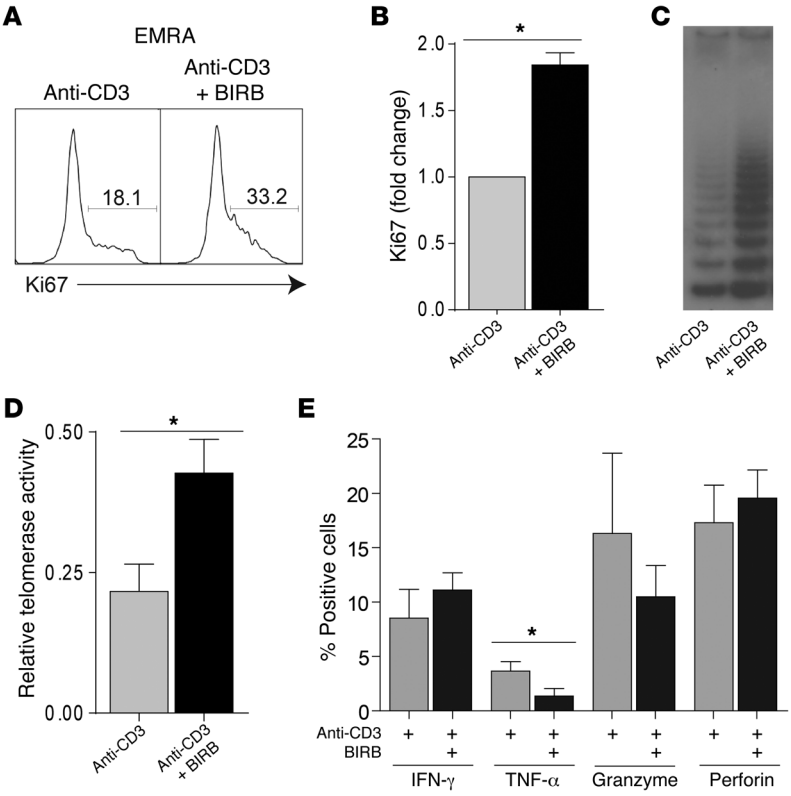

Figure 4. Signaling through p38 MAPK pathways contribute to reduced proliferation and telomerase activity of EMRA CD8⁺ T cells. (**A**) Representative example of Ki67 staining on EMRA CD8⁺ T cells measured after 3 days of stimulation with 0.5 μg/ml anti-CD3 and 5 ng/ml IL-2 in the presence or absence of 500 nM BIRB 796. Numbers depict percent Ki67⁺ cells. (**B**) Effect of BIRB 796 on proliferation of EMRA CD8⁺ T cells activated as in **A** (n = 5). (**C** and **D**) Representative blot (**C**) and data (**D**) showing telomerase activity in EMRA CD8⁺ T cells on day 3 after activation as in **A** (n = 4). (**E**) Expression of IFN-γ, TNF-α, granzyme, and perforin in EMRA CD8⁺ T cells after an 8-hour stimulation with 0.5 μg/ml anti-CD3 (n = 5). *P < 0.05, paired t test.

sets (Figure 6E). Relocalization of LC3 puncta to autophagosomal membranes and increased lysosomal content are both hallmarks of autophagy (29). Detection of autophagy should measure both of these as well as delivery of LC3 to the lysosomes (reflected by the colocalization of LC3 and lysosomal markers). The fluorescence intensity of both endogenous LC3 and the lysosomal marker Lyso-ID, along with their colocalization index (bright detail similarity; BDS), can be detected using ImageStream technology, as previously described by Phadwal and colleagues (29). Using this method, we found that after a 2-hour stimulation, EMRA CD8⁺ T cells displayed low levels of autophagy, as shown by the BDS^{hi} percentage among double-positive cells (Figure 6, E and G). However, when stimulated in the presence of BIRB 796, these cells showed the highest increase in autophagic activity (Figure 6, F and G).

We next investigated how the increase in autophagic activity was regulated. The inhibitory activity of mTORC1 on autophagy has been well documented, and its activity reflects cellular nutritional status (30). We found that expression of phosphorylated S6 (pS6; a downstream effector of mTORC1) decreased progressively, from naive to CM to EM, with the EMRA subset expressing very little pS6 ribosomal protein after stimulation (Figure 7, A and B). This result was not simply a difference in the kinetics of pS6 in the EMRA subset: over the course of a 12-hour period, the level of pS6 did not change (Supplemental Figure 3A), pointing to a lack of involvement of mTORC1 in regulating autophagy in these cells. These findings were confirmed using ImageStream technology, after a 2-hour stimulation with or without the mTORC1 inhibitor rapamycin (Figure 7C). EMRA CD8⁺ T cells were the only subset that did not display an increase in autophagic activity in the presence of rapamycin, as demonstrated by the unchanged BDS^{hi} ratio among LC3 and Lyso-ID double-positive cells (Figure 7D). Further verification that mTORC1 was not involved in EMRA CD8⁺ T cells came from the inclusion of BIRB 796, where EMRA CD8⁺ T cells showed no change in pS6 (Supplemental Figure 3, B and C), and from siRNA-mediated knockdown of MK2. The knockdown of this downstream kinase of p38 MAPK, which enhances mTORC1 (31), was found to decrease pS6 in naive, CM, and EM CD8⁺ T cells, but not the EMRA population (Supplemental Figure 3, D–F). Thus, autophagy is not regulated by mTORC1 signaling in EMRA CD8⁺ T cells.

Our findings strongly suggest that p38 MAPK inhibits autophagy and that blocking this kinase enables the use of the degraded cellular proteins and organelles, in order to provide EMRA CD8⁺ T cells with an additional energy source via an mTORC1-independent mechanism.

p38 MAPK controls autophagy in EMRA CD8⁺ T cells by regulating the p38IP-ATG9 interaction. To further understand how p38 MAPK regulates autophagy, we investigated the role of p38 interacting protein (p38IP), a protein that binds both p-p38 MAPK and autophagy protein 9 (ATG9), a key transmembrane protein required for trafficking during autophagy (32). ATG9 has been shown to localize to the *trans*-Golgi network (TGN) and late endosomes, where it enables autophagy, with p38IP regulating this trafficking (33). P-p38 can inhibit the trafficking of ATG9, as it has a higher binding affinity for p38IP than ATG9. We therefore investigated whether p38 MAPK regulates autophagy in the EMRA subset by preventing the interaction between ATG9 and p38IP. Using ImageStream, we found that after a 2-hour stimulation in the presence of BIRB 796, the amount of ATG9 colocalized with TGN markedly decreased, whereas colocalization of ATG9 with late

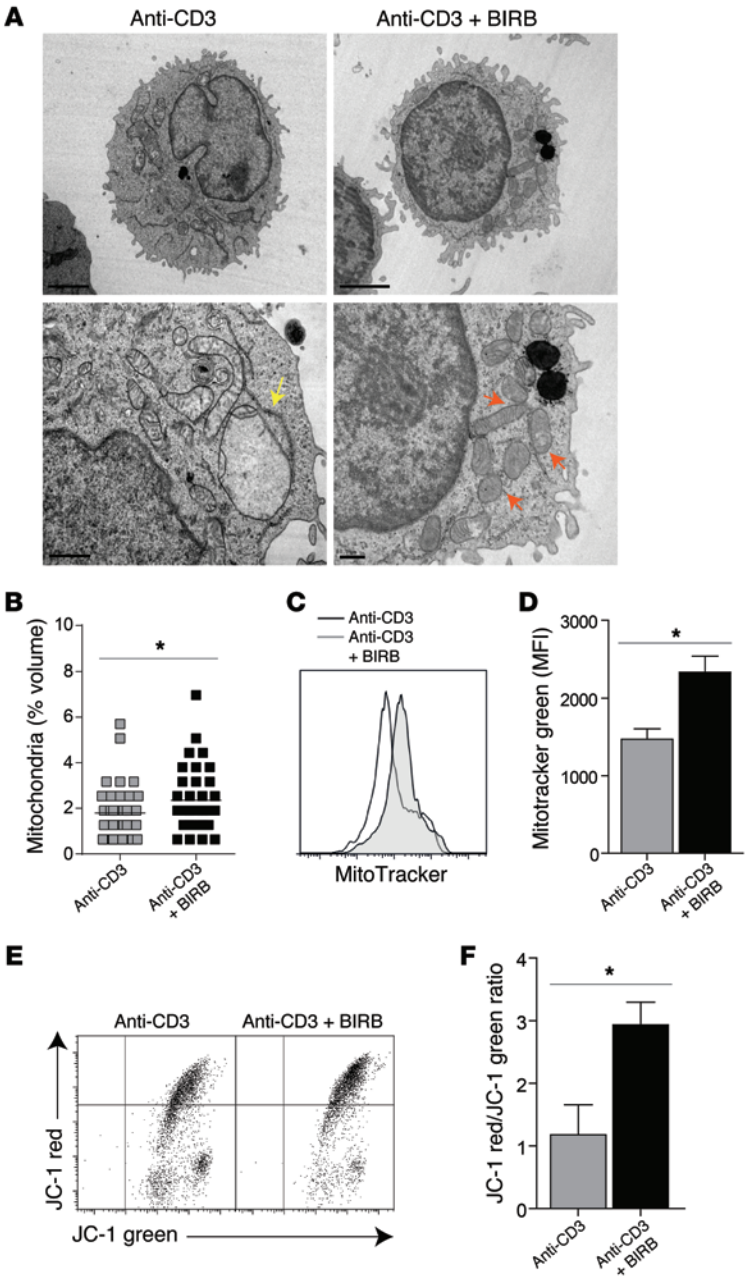

Figure 5. Inhibiting p38 MAPK pathways reverses mitochondrial dysfunction in EMRA CD8⁺ T cells. EMRA CD8⁺ T cells were stimulated for 3 days with 0.5 μg/ml anti-CD3 and 5 ng/ml IL-2 plus either 0.1% DMSO or 500 nM BIRB 796. (**A**) Electron microscope images. Scale bars: 2 μM (top); 1 μM (bottom left); 0.5 μM (bottom right). (**B**) Percentage by cell volume of mitochondria, determined by a point counting grid method from 50 different electron microscope images. (**C** and **D**) Representative example (**C**) and data (**D**) showing expression of Mitotracker Green ($n = 5$). (**E** and **F**) Example (**E**) and data (**F**) showing JC-1 staining ($n = 5$). *$P < 0.05$, paired t test.

endosomes increased, thus facilitating autophagy (Figure 8, A–D). While LAMP1 also marks lysosomes and autolysosomes, we demonstrated here that inhibition of p38 MAPK signaling alters the trafficking of ATG9. The effect of BIRB 796 on ATG9 trafficking was only observed in the EMRA subset (Figure 8, E and F), which suggests that p38 MAPK negatively regulates the p38IP-ATG9 interaction and prevents redistribution of ATG9 to the endosomes controlling the level of autophagy.

Discussion

The paradigm of cellular senescence has mainly been defined in stromal cells such as fibroblasts that grow in vitro (19, 34). Although senescence-like characteristics have also been described in primary human T lymphocytes, this has largely been based on analysis of whole-lymphocyte fractions (35, 36). Furthermore, while many publications have investigated either the cell signaling processes or the functional activity of the senescent subpopulation, the majority of these have used loss of CD28 expression as a marker of senescence (10, 11). We previously found that while EMRA CD8⁺ T cells are all CD28⁻, the majority of EM CD8⁺ T cells, which do not exhibit functional characteristics of senescence, are also CD28⁻ (20). In order to obtain a more complete definition of primary human T cell senescence, we performed an extensive phenotypic and functional analysis of the senescence characteristics of freshly isolated human CD8⁺ T cells that were identified at different stages of differentiation by their relative expression of CD45RA and CD27. After T cell activation, the EMRA CD8⁺ T cell population ($CD45RA^+CD27^-$) had reduced proliferative capacity, together with low telomerase expression, extensive expression of DNA damage foci, and activation of the key senescence-signaling molecule p38 MAPK, all of which were indicative of senescence rather than quiescence. Furthermore, the loss of mTOR in EMRA CD8⁺ T cells was also indicative of senescence, as mTOR activity has been shown to enforce quiescence (37). These cells also expressed high levels of CD57 and KLRG1 and low levels of CD28, considered to be a characteristic of senescent T cells (7, 9). However, EM CD8⁺ T cells ($CD45RA^-CD27^-$) also expressed high levels of CD57 and KLRG1 and low levels of CD28, like the EMRA population, but could proliferate and express telomerase activity after activation, which indicates that they are not a senescent population. Although loss of CD28 expression is a feature of exhausted human CD8⁺ T cells (38), EMRA CD8⁺ T cells were not functionally exhausted, as they retained cytotoxic capability and produced high levels of IFN-γ and TNF-α; furthermore, they only expressed low levels of key markers of exhaustion, such as PD-1 (39, 40). Additionally, EMRA CD8⁺ T cells had a lower turnover than effectors; however, the rate of death/disappearance of this subset was decreased, implying that it represents a long-lived pool of cells that persist in the circulation (41).

The senescent characteristics of EMRA CD8⁺ T cells may not be induced by telomere erosion alone (42). Although these cells have shorter telomeres than naive CD8⁺ T cells, they have significantly longer telomeres than the EM subpopulation. Senescence can also be induced by damage by ROS (1). We found that EMRA CD8⁺ T cells expressed high levels of both mitochondrial and cytoplasmic ROS, exhibited large dysfunctional mitochondria

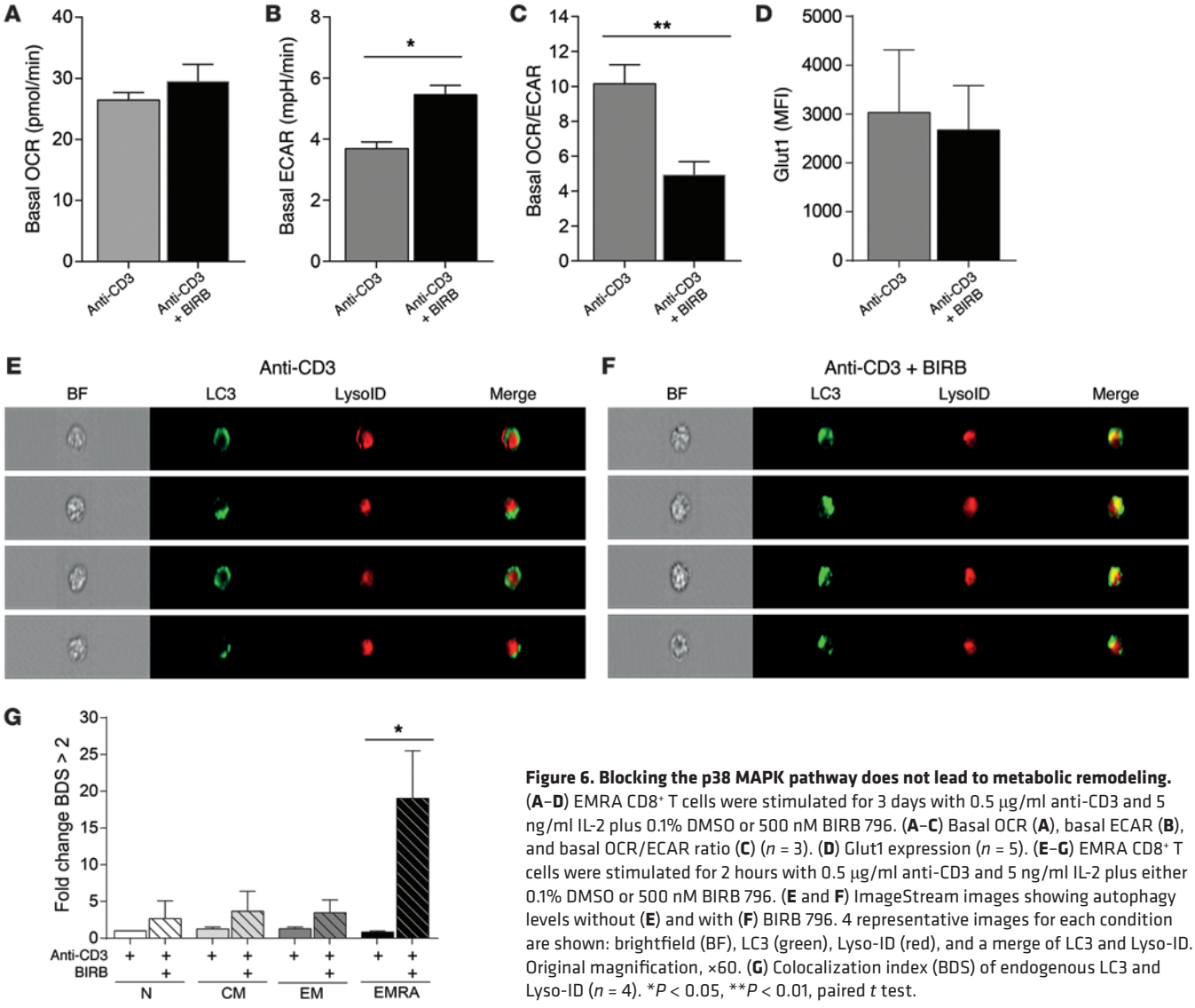

Figure 6. Blocking the p38 MAPK pathway does not lead to metabolic remodeling. (**A**–**D**) EMRA CD8⁺ T cells were stimulated for 3 days with 0.5 μg/ml anti-CD3 and 5 ng/ml IL-2 plus 0.1% DMSO or 500 nM BIRB 796. (**A**–**C**) Basal OCR (**A**), basal ECAR (**B**), and basal OCR/ECAR ratio (**C**) (n = 3). (**D**) Glut1 expression (n = 5). (**E**–**G**) EMRA CD8⁺ T cells were stimulated for 2 hours with 0.5 μg/ml anti-CD3 and 5 ng/ml IL-2 plus either 0.1% DMSO or 500 nM BIRB 796. (**E** and **F**) ImageStream images showing autophagy levels without (**E**) and with (**F**) BIRB 796. 4 representative images for each condition are shown: brightfield (BF), LC3 (green), Lyso-ID (red), and a merge of LC3 and Lyso-ID. Original magnification, ×60. (**G**) Colocalization index (BDS) of endogenous LC3 and Lyso-ID (n = 4). *P < 0.05, **P < 0.01, paired t test.

with little or no cristae, and had a lower MMP. This is in line with studies reporting that aging cells show accumulation of giant or highly interconnected mitochondria, characterized by loss of cristae structure and swollen morphology (43).

Decreased mitochondrial function in aged liver and muscle cells has been shown to result in a decline in energy production, causing metabolic reprogramming toward extramitochondrial energy production (25). We showed here that senescent CD8⁺ T cells also adopted anaerobic glycolysis instead of OXPHOS to produce energy. Mitochondrial dysfunction may also be a reason why highly functional effector cells use glycolysis despite being less efficient than OXPHOS at generating energy, a feature that has also been reported in murine effector T cells (44). In mice, these metabolic changes in effector cells are regulated through the induction of mitochondrial biogenesis and an increased capacity to respond to metabolic stress, a characteristic quantified as SRC (28). We found the SRC to be high in early differentiated human memory CD8⁺ T cells, but substantially decreased in senescent CD8⁺ T cells. This correlated with the changes in mitochondrial mass: it was higher in the CM and EM subsets, conferring a bioenergetic advantage, whereas in senescent cells, mitochondrial content was markedly reduced and the mitochondrial membrane hyperpolarized, leading to increased ROS production.

Previous studies have shown that EMRA CD8⁺ T cells preferentially localize to peripheral organs, where they may have to perform their effector functions under hypoxic conditions (45), suggestive of a link among metabolism, migration, and effector function (46). Our present results extended this concept by showing that highly functional senescent CD8⁺ T cells that have the typical glycolytic pathway dependence of cytotoxic effector cells may represent a senescent population. This raises the possibility that senescence signaling, cellular metabolism and effector function are regulated in tandem in these cells. EMRA CD8⁺ T cells had very potent effector function despite their mitochondrial dysfunction, raising the question of whether the energy required for proliferation is sacrificed to ensure that cytotoxic activity and cytokine secretion can take place. EM CD8⁺ T cells, which also have potent cytotoxic potential and secrete cytokines, can also proliferate; however, in contrast to the senescent EMRA population, these cells can utilize both OXPHOS and aerobic glycolysis. This extends the emerging

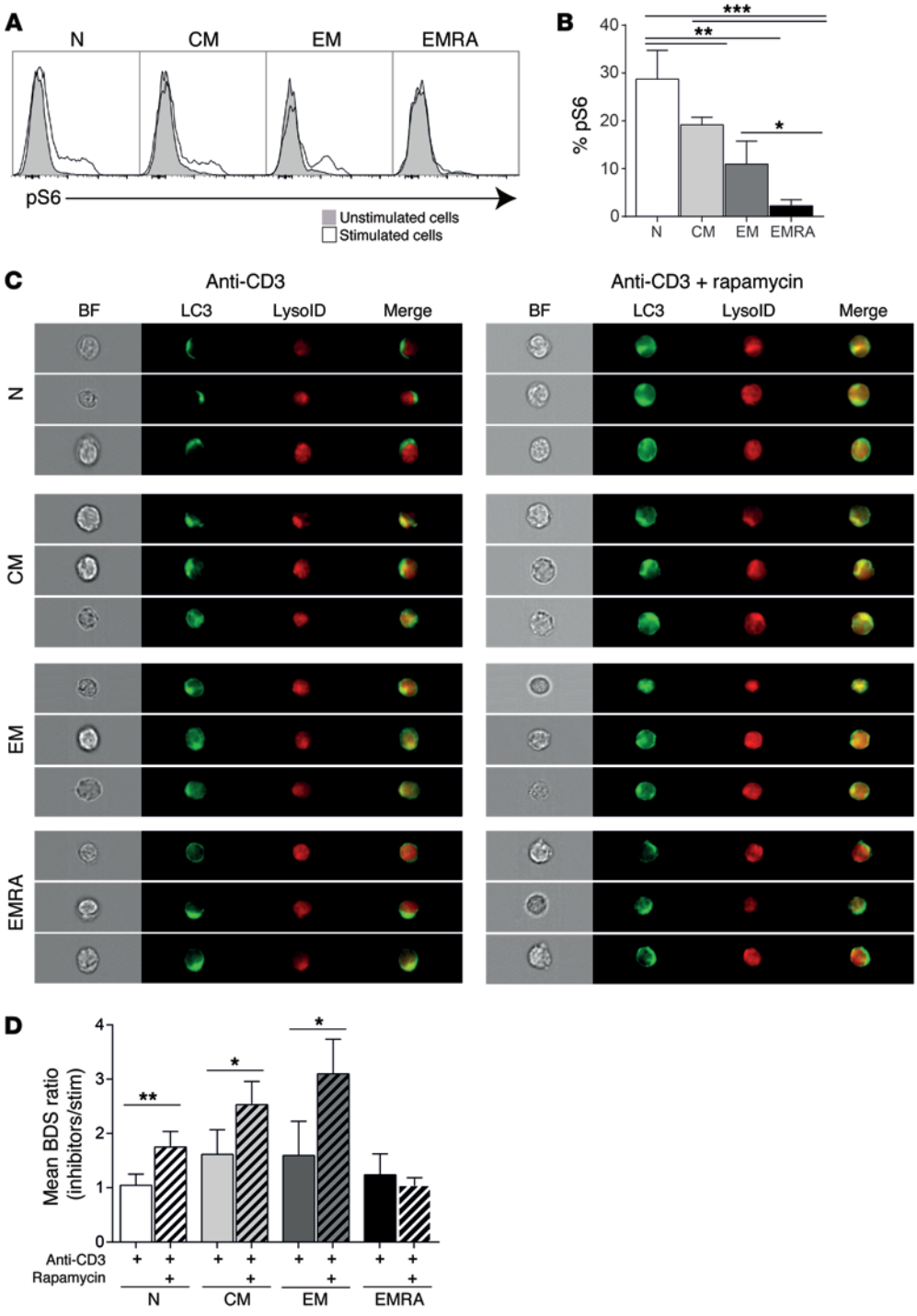

Figure 7. Increased autophagic activity in EMRA CD8⁺ T cells is achieved via an mTORC1-independent mechanism. (**A** and **B**) Example (**A**) and data (**B**) of pS6 within the CD8⁺ T cell subsets following a 2-hour stimulation with 0.5 μg/ml anti-CD3 (n = 5). (**C** and **D**) CD8⁺ T cell subsets were stimulated for 2 hours with 0.5 μg/ml anti-CD3 and 5 ng/ml IL-2 plus either 0.1% DMSO or 100 nM rapamycin. (**C**) ImageStream images showing autophagy levels. 4 representative images for each condition are shown: brightfield, LC3 (green), Lyso-ID (red), and a merge of LC3 and Lyso-ID. Original magnification, ×60. (**D**) Colocalization index (BDS) of endogenous LC3 and Lyso-ID (n = 4). $^*P < 0.05$, $^{**}P < 0.01$, $^{***}P < 0.001$, repeated-measures ANOVA followed by Tukey correction.

data from mouse models showing that effector CD8⁺ T cells maintain OXPHOS in conjunction with glycolysis (28).

In a previous study, it was shown that p38 blockade could increase the proliferation and telomerase activity of highly differentiated CD4⁺ T cells (13). We therefore investigated whether inhibition of p38 MAPK, expression of which was elevated in senescent CD8⁺ T cells, could increase proliferation and alter the metabolism of the cell after activation. We showed here that blocking p38 MAPK caused an increase in mitochondrial mass and improved mitochondrial function, which translated to an enhanced proliferative capacity. This raised the question of whether these cells now switched their metabolism to OXPHOS to supply the extra energy demands for cell cycling. Instead, we found that these cells still preferentially engaged glycolysis; however, this was not associated with an increased uptake of glucose, as expression of the glucose transporter Glut1 remained unchanged in the senescent CD8⁺ T cells both with and without addition of BIRB 796 during activation.

Autophagy can generate metabolic precursors from lysosomal digestion of organelles and other materials for metabolism (47). Furthermore, mouse models have shown that autophagy supports glycolysis and that autophagy competence is required for cells to proliferate and expand (48). We found that senescent CD8⁺ T cells

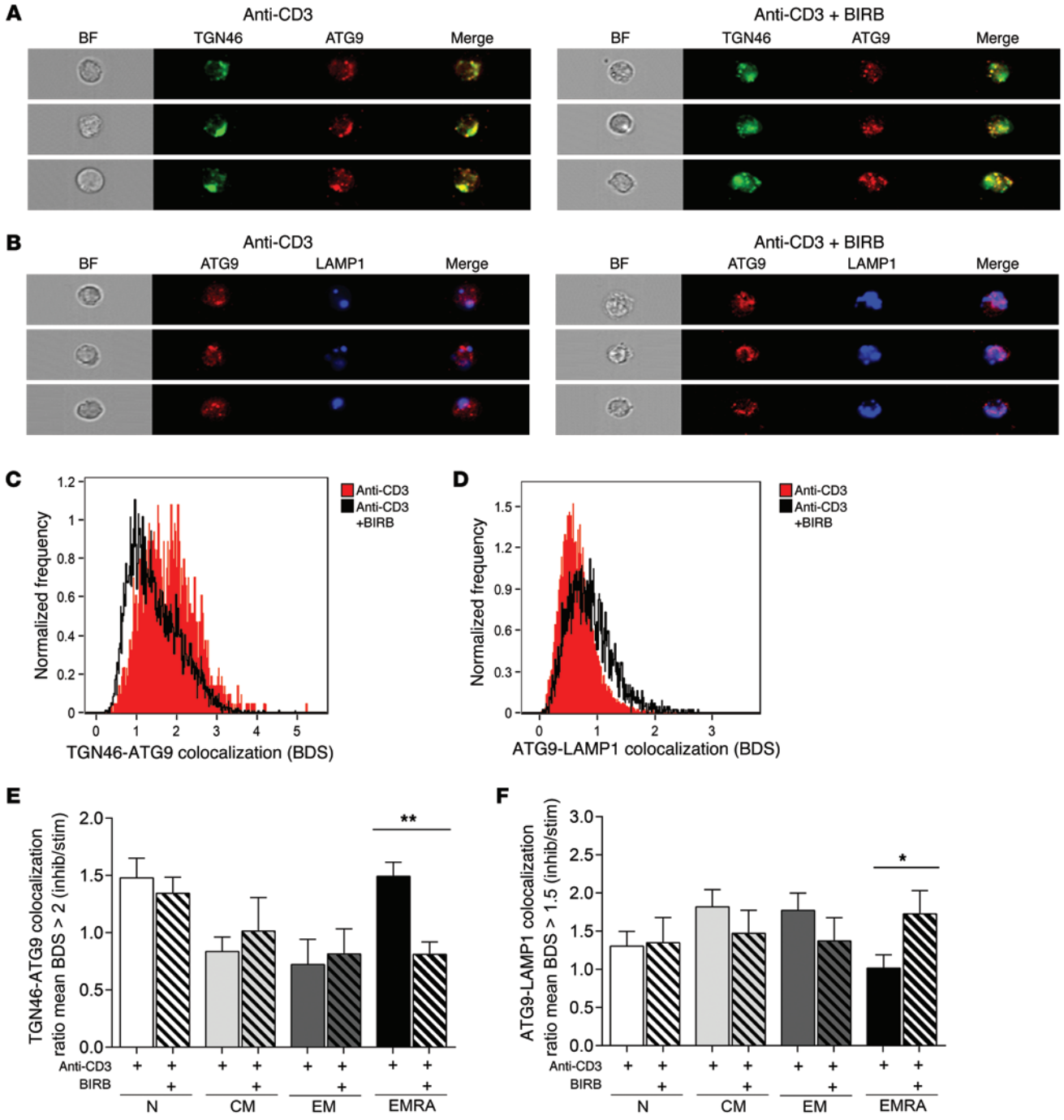

Figure 8. p38 MAPK controls autophagy in EMRA CD8⁺ T cells by regulating the p38IP-ATG9 interaction. EMRA CD8⁺ T cells were stimulated for 2 hours with 0.5 μg/ml anti-CD3 and 5 ng/ml IL-2 plus either 0.1% DMSO or 500 nM BIRB 796. (**A**) ImageStream images showing colocalization of ATG9 with TGN46. 4 representative images per condition are shown: brightfield, TGN46 (green), ATG9 (red), and a merge of TGN46 and ATG9. (**B**) Colocalization of ATG9 with LAMP1. 4 representative images per condition are shown: brightfield, ATG9 (red), LAMP1 (blue), and a merge of ATG9 and LAMP1. Original magnification, ×60 (**A** and **B**). (**C** and **D**) Representative BDS overlay histogram of EMRA CD8⁺ T showing colocalization of TGN46 and ATG9 (**C**) and of LAMP1 and ATG9 (**D**). Colocalization index (BDS) of TGN46 and ATG9 (**E**) and of LAMP1 and ATG9 (**F**) ($n = 4$). *$P < 0.05$, **$P < 0.01$, repeated-measures ANOVA followed by Tukey correction.

displayed low autophagic activity, in line with a previous report investigating $CD8^+CD28^-CD57^+$ T cells (29). The absence of key autophagy genes has been shown to increase both ROS and damage to the lymphoid mitochondria (49), linking mitochondrial oxidative stress with autophagy (29). A key finding was that p38 blockade in EMRA CD8⁺ T cells induced a considerable increase in autophagy, allowing for the increased biosynthesis in these cells.

We found that p38 MAPK inhibited autophagy in an mTOR-independent manner. The observed reduction in phosphorylation of the S6 ribosomal protein, a surrogate marker for mTORC1

activation, declined during differentiation from the naive to the EMRA subset. This is in line with reports that the transition to a memory phenotype is associated with a metabolic switch from anabolism to catabolism (46, 50) via inhibition of mTOR (51). We have also previously shown that highly differentiated CD8$^+$ T cells lack the ability to phosphorylate Akt (21), an upstream activator of mTORC1, which suggests that the PI3K/Akt/mTOR pathway does not play a role in senescent T cells. We postulate here that autophagy is regulated in EMRA CD8$^+$ T cells via p38 MAPK independently of mTOR, in part by the preferential binding of p-p38 MAPK to p38IP compared with that of ATG9 to p38IP, thereby regulating the trafficking and function of ATG9. It is now becoming apparent that there are a variety of noncanonical pathways leading to autophagosomal degradation through variants of the canonical pathway (52). Indeed, the existence of noncanonical forms of autophagy that can bypass the AMPK-mTOR-ULK1 circuit of initiation have been documented (53). Furthermore, Beclin 1–independent autophagy was observed where ROS and/or mitochondrial damage are involved (54), with ATG9 being independently recruited to depolarized mitochondria (55). Here, we described a novel subset-specific noncanonical mechanism whereby p-p38 MAPK negatively regulates autophagy in the EMRA CD8$^+$ T cells.

Collectively, our results suggest that some aspects of senescence in human CD8$^+$ T cells are mediated by p38 MAPK signaling and are reversible. We postulate that inhibition of p38 MAPK increases autophagy, releasing metabolic precursors and allowing the cell to increase its proliferative capacity. Proliferation was only increased in the EMRA subset, either directly or indirectly through the removal of p53, as p38 plays a key role in its phosphorylation and activation (3). Senescent T cells closely resembled the classically defined short-lived effector T cells that arise during an immune response; however, EM CD8$^+$ T cells also had effector function, but were not senescent. Both these populations of effector cells were very different metabolically and used different pathways to generate energy, which were not governed by p38 MAPK signaling. This reversibility of the senescent CD8$^+$ phenotype is important, as the number of EMRA CD8$^+$ T cells increases considerably during aging (20) as well as in patients with autoimmune diseases (56), malignancy (57), and persistent infections (58). Finally, it remains unanswered whether reestablishment of proliferative activity in senescent CD8$^+$ T cells by p38 blockade may improve immune responsiveness in these subjects.

Methods

Blood sample collection and isolation. Heparinized peripheral blood samples were taken from young, healthy volunteers (age range, 20–35 years; median, 31 years; n = 62). Healthy was taken as individuals who had not had an infection or immunization within the last month, had no known immunodeficiency or any history of chemotherapy or radiotherapy, and were not receiving systemic steroids within the last month or any other immunosuppressive medications within the last 6 months. PBMCs were isolated using Ficoll hypaque (Amersham Biosciences) and either analyzed immediately or cryopreserved as described previously (8).

Flow cytometric analysis and cell sorting. Flow cytometric analysis was performed using the following antibodies (all from BD Biosciences, unless otherwise specified): live/dead fixable blue dead cell stain (Invitrogen), KLRG1 PE (13F12; gift from H. Pircher, University of Freiburg, Freiburg, Germany), CD45RA Brilliant Violet 605 (Biolegend), Via Probe, CD8 PerCP (SK1), CD8 Alexa Fluor 700 (RPA-T8), CD27 FITC (M-T271), CD27 APC-H7 (M-T271), CD45RA PE-Cy7 (L48), and CD57 APC (NK-1). For intracellular staining, the following antibodies were used (all from BD Biosciences, unless otherwise specified): pS6 ribosomal protein (Ser235/236, D457.2.2E; Cell Signaling), IFN-γ V450 (B27), granzyme B Alexa Fluor 700 (GB11), TNF-α PE (MAb11), perforin FITC (ΔG9), and p-p38 Alexa Fluor 488 (36/p38). Intranuclear staining was performed using γH2AX Alexa Fluor 488 (2F3; Biolegend) and Ki67 FITC (B56; BD Biosicences). All samples were run using an LSR II (BD Biosciences) and analyzed using FlowJo software (Treestar).

CD8$^+$ T cells were purified by positive selection using the VARIOMACS system (MiltenyiBiotec) according to the manufacturer's instructions. Positively selected CD8$^+$ T cells were labeled with CD27 FITC (M-T271; BD Biosciences) and CD45RA APC (HI100; BD Biosciences) and sorted using a FACSAria (BD Biosciences). The purity of CD8$^+$ T cell subsets was assessed by flow cytometry. Multiparamter flow cytometry was analyzed, and presentation of distributions was performed using SPICE version 5.2 (http://exon.niaid.nih.gov/spice/; ref. 59).

Phosphoflow cytometry. Analysis of p-p38 (pT180/pY182) was performed after a 30-minute stimulation with 0.5 μg/ml PMA/ionomycin. Following surface staining for CD45RA, CD27, and CD8, PBMCs were fixed with warm Cytofix Buffer (BD Biosciences). Cells were then permeabilized with ice-cold Perm Buffer III (BD Biosciences) and incubated with the anti-p38 antibody (pT180/pY182) for 30 minutes at room temperature. For the detection of γH2AX (pS139), purified subsets were activated with 0.5 μg/ml plate coated anti-CD3 (OKT3) and 5 ng/ml of rhIL-2 (Peprotech) overnight, pS6 ribosomal protein (Ser235/236, D57.2.2E, Cell Signaling) was measured following a 2-hour stimulation with 0.5 μg/ml plate coated anti-CD3 (OKT3), after which the above staining method was used.

Western blot analysis. Cell lysates were made from sorted CD45RA/CD27 CD8$^+$ T cell subsets by sonication in 50 mM Tris-HCl (pH 7.5), 2 mM EGTA, and 0.1% Triton X-100 buffer. Lysates from 1×10^6 cells were fractionated by SDS–polyacrylamide electrophoresis and analyzed by immunoblotting with p-p38 MAPK (12F8; Cell Signalling), using the ECL Advanced Western Blotting Detection Kit (GE Healthcare) according to the protocol provided by the manufacturer.

Proliferation assays. CD45RA/CD27-sorted CD8$^+$ T cells were stimulated with 0.5 μg/ml plate coated anti-CD3 (OKT3) and 5 ng/ml IL-2 for 3 days, and proliferation was assessed by staining for the cell cycle–related nuclear antigen Ki67 as described previously (8).

Mitochondrial measurements. For all mitochondrial experiments, freshly isolated PBMCs were first surface stained using Via Probe, CD8 Alexa Fluor 700, CD27 APC (BD Biosciences), and CD45RA Brilliant Violet 605 (Biolegend). For assessment of mitochondrial mass, the labeled PBMCs were incubated with 100 nM MitoTracker Green FM (Invitrogen) for 30 minutes at 37°C, 5% CO_2. MMP was investigated using JC-1 (Invitrogen); 2 μM JC-1 was incubated with labeled PBMCs for 30 minutes at 37°C, 5% CO_2. Addition of 100 μM CCCP was used to confirm that the JC-1 response was sensitive to changes in MMP. Unfixed samples were immediately collected on a LSR II (BD Bioscience).

Relative quantification of mtDNA copy number was performed by extracting genomic DNA using the QIAamp DNA kit (Qiagen). The

resulting DNA was used to determine mtDNA/nDNA ratios by real-time PCR using primers against NADH dehydrogenase I and beta-2 microglobulin using the Applied Biosystems 7500 sequence detection system. The expression of mtDNA for genes of interest was normalized to the expression of the housekeeping gene (B2M).

Transmission electron microscopy studies. Naive, CM, EM, and EMRA CD8$^+$ T cells were isolated and stimulated with anti-CD3 (OKT3; 0.5 μg/ml) and 5 ng/ml IL-2 (Peprotech) for 3 days, with or without the p38 MAPK inhibitor BIRB 796. The cells were fixed in 2% paraformaldehyde, 1.5% glutaraldehyde with 0.1 m phosphate buffer (pH 7.3). They were then osmicated in 1% OsO_4 with 0.1 m phosphate buffer, dehydrated in a graded ethanol-water series, cleared in propylene oxide, and infiltrated with Araldite resin. Ultrathin sections were cut using a diamond knife, collected on 300 mesh grids, and stained with uranyl acetate and lead citrate. Cells were viewed in a Jeol 1010 transmission electron microscope (Jeol) and imaged using a Gatan Orius CCD camera (Gatan). Mitochondrial volume density (calculated as the percentage of CD8$^+$ T cell volume occupied by mitochondria) was determined from electron microscopic images using a point-counting method with a grid generated by Image J: the grid was drawn on the image, and the number of intersection points that fell on mitochondria was determined.

Metabolic assays. OCR and ECAR were measured in the CD8$^+$ T cell subsets after stimulation with anti-CD3 and 5 ng/ml IL-2 either overnight or for 3 days, with or without 500 nM BIRB 796. The assay was performed in RPMI without phenol red and carbonate buffer (Sigma-Aldrich) containing 25 mM glucose, 2 mM L-glutamine, and 1 mM pyruvate. The metabolic stress test was performed using 1 μM oligomycin, 1.5 μM fluorocarbonyl cyanide phenylhydrazone (FCCP), 100 nM rotenone, and 1 μM antimycin A (Seahorse Bioscience) with the XF-24 Extracellular Flux Analyzer (Seahorse Bioscience).

Inhibition of p38 signaling. Signaling through p38 MAPK on sorted CD27/CD45RA-defined CD8$^+$ T cell subsets was blocked by adding the small-molecule p38 inhibitor BIRB 796, which blocks the activity of all forms of the molecule. CD8$^+$ T cell subsets were incubated with 500 nM BIRB 796 for 1 hour prior to stimulation with anti-CD3 (OKT3; 0.5 μg/ml) and 5 ng/ml rhIL-2 (13). 0.1% DMSO was used as a control.

Assessment of autophagy. Autophagy was investigated using ImageStream. PBMCs were incubated with or without BIRB 796 and the inhibitors E64d and pepstatin A (Sigma-Aldrich; 10 μg/ml each) to induce autophagy for 2 hours. Subsequently, PBMCs were stained with the lysosomal marker Lyso-ID (Enzo Life Sciences); surface stained with CD8, CD45RA, and CD27; fixed and permeabilized using eBioscience Fixation and Permeabilization kit; stained with polyclonal LC3 (MBL); and run on ImageStream. Autophagy levels were calculated by measuring percent colocalization of LC3^{hi}Lyso^{hi} CD45RA/CD27-defined CD8$^+$ T cell subsets, achieved by measuring the BDS between LC3 and lysosomal markers normalized against the frequency of cells (29).

Colocalization of ATG9 and the TGN and endosomes. Colocalization was investigated using ImageStream. PBMCs were incubated with or without BIRB 796 and the inhibitors E64d and pepstatin A (Sigma-Aldrich; 10 μg/ml each) to induce autophagy for 2 hours. Subsequently, PBMCs were surface stained with CD8, CD45RA, and CD27; fixed and permeabilized using eBioscience Fixation and Permeabilization kit; stained with ATG9 (generated as described previously; ref. 60), TGN46 (AHP500G; AbD Serotec), and CD107a (1D4B; BD Biosciences); and run on ImageStream. Colocalization was calculated by measuring percent BDS of ATG9^{hi}TGN46^{hi} or ATG9^{hi}LAMP1^{hi} CD45RA/CD27-defined CD8$^+$ T cell subsets, followed by determining the ratio of BDS in the presence and absence of the autophagy inhibitors.

Statistics. Graphpad Prism was used to perform statistical analysis. Statistical significance was evaluated using 2-tailed paired Student's *t* test or repeated-measures ANOVA with Tukey correction for post-hoc testing. Bar graphs show mean ± SEM. A *P* value less than 0.05 was considered significant.

Study approval. The present study was reviewed and approved by the ethical committee of Royal Free and University College Medical School. All subjects provided written informed consent.

Acknowledgments

We thank M. Turmaine for technical assistance with the electron microscope and J. Passos and T. von Zglinicki for help and expertise in analyzing mitochondria. This work was supported by the Biotechnology and Biological Sciences Research Council (to S.M. Henson and A.N. Akbar) and the Medical Research Council (to A. Lanna). A.K. Simon is supported by the Oxford Biomedical Research Centre, funded by the NIHR; D.J. Puleston is funded by the Wellcome Trust; A.S. Watson is funded by Lady Tata Memorial Trust; and S.A. Tooze is funded by Cancer Research UK.

Address correspondence to: Sian M. Henson, Division of Infection and Immunity, University College London, 5 University Street, London, WC1E 6JF, United Kingdom. Phone: 44.203.108.2179; E-mail: s.henson@ucl.ac.uk.

1. Campisi J, d'Adda di Fagagna F. Cellular senescence: when bad things happen to good cells. *Nat Rev Mol Cell Biol*. 2007;8(9):729–740.
2. Passos JF, Von Zglinicki T. Oxygen free radicals in cell senescence: are they signal transducers? *Free Radic Res*. 2006;40(12):1277–1283.
3. Coppe JP, et al. Senescence-associated secretory phenotypes reveal cell-nonautonomous functions of oncogenic RAS and the p53 tumor suppressor. *PLoS Biol*. 2008;6(12):2853–2868.
4. Liu K, Hodes RJ, Weng N. Cutting edge: telomerase activation in human T lymphocytes does not require increase in telomerase reverse transcriptase (hTERT) protein but is associated with hTERT phosphorylation and nuclear translocation. *J Immunol*. 2001;166(8):4826–4830.
5. Plunkett FJ, et al. The impact of telomere erosion on memory CD8$^+$ T cells in patients with X-linked lymphoproliferative syndrome. *Mech Ageing Dev*. 2005;126(8):855–865.
6. van de Berg PJ, et al. Cytomegalovirus infection reduces telomere length of the circulating T cell pool. *J Immunol*. 2010;184(7):3417–3423.
7. Brenchley JM, et al. Expression of CD57 defines replicative senescence and antigen-induced apoptotic death of CD8$^+$ T cells. *Blood*. 2003;101(7):2711–2720.
8. Henson SM, et al. KLRG1 signaling induces defective Akt (ser473) phosphorylation and proliferative dysfunction of highly differentiated CD8$^+$ T cells. *Blood*. 2009;113(26):6619–6628.
9. Voehringer D, Koschella M, Pircher H. Lack of proliferative capacity of human effector and memory T cells expressing killer cell lectinlike receptor G1 (KLRG1). *Blood*. 2002;100(10):3698–3702.
10. Dagarag M, Evazyan T, Rao N, Effros RB. Genetic manipulation of telomerase in HIV-specific CD8$^+$ T cells: enhanced antiviral functions accompany the increased proliferative potential and telomere length stabilization. *J Immunol*. 2004;173(10):6303–6311.
11. Scheuring UJ, Sabzevari H, Theofilopoulos AN. Proliferative arrest and cell cycle regulation in CD8(+)CD28(–) versus CD8(+)CD28(+) T cells. *Hum Immunol*. 2002;63(11):1000–1009.
12. Lunt SY, Vander Heiden MG. Aerobic glycolysis: meeting the metabolic requirements of cell prolif-

eration. *Annu Rev Cell Dev Biol*. 2011;27:441–464.
13. Di Mitri D, et al. Reversible senescence in human CD4+CD45RA+CD27- memory T cells. *J Immunol*. 2011;187(5):2093–2100.
14. Chang L, Karin M. Mammalian MAP kinase signalling cascades. *Nature*. 2001;410(6824):37–40.
15. Salvador JM, et al. Alternative p38 activation pathway mediated by T cell receptor-proximal tyrosine kinases. *Nat Immunol*. 2005;6(4):390–395.
16. Freund A, Patil CK, Campisi J. p38MAPK is a novel DNA damage response-independent regulator of the senescence-associated secretory phenotype. *EMBO J*. 2011;30(8):1536–1548.
17. Appay V, van Lier RA, Sallusto F, Roederer M. Phenotype and function of human T lymphocyte subsets: consensus and issues. *Cytometry A*. 2008;73(11):975–983.
18. Akbar AN, Henson SM. Are senescence and exhaustion intertwined or unrelated processes that compromise immunity? *Nat Rev Immunol*. 2011;11(4):289–295.
19. d'Adda di Fagagna F, et al. A DNA damage checkpoint response in telomere-initiated senescence. *Nature*. 2003;426(6963):194–198.
20. Koch S, Larbi A, Derhovanessian E, Ozcelik D, Naumova E, Pawelec G. Multiparameter flow cytometric analysis of CD4 and CD8 T cell subsets in young and old people. *Immun Ageing*. 2008;5:6.
21. Plunkett FJ, et al. The loss of telomerase activity in highly differentiated CD8+CD28-CD27- T cells is associated with decreased Akt (Ser473) phosphorylation. *J Immunol*. 2007;178(12):7710–7719.
22. Romero P, et al. Four functionally distinct populations of human effector-memory CD8+ T lymphocytes. *J Immunol*. 2007;178(7):4112–4119.
23. Iwasa H, Han J, Ishikawa F. Mitogen-activated protein kinase p38 defines the common senescence-signalling pathway. *Genes Cells*. 2003;8(2):131–144.
24. Petrovas C, et al. Increased mitochondrial mass characterizes the survival defect of HIV-specific CD8(+) T cells. *Blood*. 2007;109(6):2505–2513.
25. Houtkooper RH, et al. The metabolic footprint of aging in mice. *Sci Rep*. 2011;1:134.
26. MacIver NJ, Michalek RD, Rathmell JC. Metabolic regulation of T lymphocytes. *Annu Rev Immunol*. 2013;31:259–283.
27. Hill BG, et al. Integration of cellular bioenergetics with mitochondrial quality control and autophagy. *Biol Chem*. 2012;393(12):1485–1512.
28. Everts B, Chang C-H, Amiel E. Mitochondrial respiratory capacity is a critical regulator of CD8+ T cell memory development. *Immunity*. 2012;36(1):68–78.
29. Phadwal K, et al. A novel method for autophagy detection in primary cells: impaired levels of macroautophagy in immunosenescent T cells. *Autophagy*. 2012;8(4):677–689.
30. Kim J, Kundu M, Viollet B, Guan KL. AMPK and mTOR regulate autophagy through direct phosphorylation of Ulk1. *Nat Cell Biol*. 2011;13(2):132–141.
31. Gaestel M. MAPKAP kinases — MKs — two's company, three's a crowd. *Nat Rev Mol Cell Biol*. 2006;7(2):120–130.
32. Webber JL, Tooze SA. New insights into the function of Atg9. *FEBS letters*. 2010;584(7):1319–1326.
33. Webber JL, Tooze SA. Coordinated regulation of autophagy by p38alpha MAPK through mAtg9 and p38IP. *EMBO J*. 2010;29(1):27–40.
34. Beausejour CM, et al. Reversal of human cellular senescence: roles of the p53 and p16 pathways. *EMBO J*. 2003;22(16):4212–4222.
35. Song Z, et al. Lifestyle impacts on the aging-associated expression of biomarkers of DNA damage and telomere dysfunction in human blood. *Aging Cell*. 2010;9(4):607–615.
36. Roth A, Baerlocher GM, Schertzer M, Chavez E, Duhrsen U, Lansdorp PM. Telomere loss, senescence, and genetic instability in CD4+ T lymphocytes overexpressing hTERT. *Blood*. 2005;106(1):43–50.
37. Yang K, Neale G, Green DR, He W, Chi H. The tumor suppressor Tsc1 enforces quiescence of naive T cells to promote immune homeostasis and function. *Nat Immunol*. 2011;12(9):888–897.
38. Riley JL, June CH. The road to recovery: translating PD-1 biology into clinical benefit. *Trends Immunol*. 2007;28(2):48–50.
39. Henson SM, Macaulay R, Franzese O, Akbar AN. Reversal of functional defects in highly differentiated young and old CD8 T cells by PDL blockade. *Immunology*. 2012;135(4):355–363.
40. Wherry EJ, et al. Molecular signature of CD8+ T cell exhaustion during chronic viral infection. *Immunity*. 2007;27(4):670–684.
41. Wallace DL, et al. Direct measurement of T cell subset kinetics in vivo in elderly men and women. *J Immunol*. 2004;173(3):1787–1794.
42. Hodes RJ, Hathcock KS, Weng NP. Telomeres in T and B cells. *Nat Rev Immunol*. 2002;2(9):699–706.
43. Seo AY, Joseph AM, Dutta D, Hwang JC, Aris JP, Leeuwenburgh C. New insights into the role of mitochondria in aging: mitochondrial dynamics and more. *J Cell Sci*. 2010;123(pt 15):2533–2542.
44. Cham CM, Gajewski TF. Glucose availability regulates IFN-gamma production and p70S6 kinase activation in CD8+ effector T cells. *J Immunol*. 2005;174(8):4670–4677.
45. Faint JM, et al. Memory T cells constitute a subset of the human CD8+CD45RA+ pool with distinct phenotypic and migratory characteristics. *J Immunol*. 2001;167(1):212–220.
46. Finlay D, Cantrell DA. Metabolism, migration and memory in cytotoxic T cells. *Nat Rev Immunol*. 2011;11(2):109–117.
47. Altman BJ, et al. Autophagy provides nutrients but can lead to Chop-dependent induction of Bim to sensitize growth factor-deprived cells to apoptosis. *Mol Biol Cell*. 2009;20(4):1180–1191.
48. Lock R, et al. Autophagy facilitates glycolysis during Ras-mediated oncogenic transformation. *Mol Biol Cell*. 2011;22(2):165–178.
49. Mortensen M, et al. Loss of autophagy in erythroid cells leads to defective removal of mitochondria and severe anemia in vivo. *Proc Natl Acad Sci U S A*. 2010;107(2):832–837.
50. Powell JD, Pollizzi KN, Heikamp EB, Horton MR. Regulation of immune responses by mTOR. *Annu Rev Immunol*. 2012;30:39–68.
51. Araki K, et al. mTOR regulates memory CD8 T-cell differentiation. *Nature*. 2009;460(7251):108–112.
52. Codogno P, Mehrpour M, Proikas-Cezanne T. Canonical and non-canonical autophagy: variations on a common theme of self-eating? *Nat Rev Mol Cell Biol*. 2012;13(1):7–12.
53. Yamamoto A, Cremona ML, Rothman JE. Autophagy-mediated clearance of huntingtin aggregates triggered by the insulin-signaling pathway. *J Cell Biol*. 2006;172(5):719–731.
54. Chu CT, Zhu J, Dagda R. Beclin 1-independent pathway of damage-induced mitophagy and autophagic stress: implications for neurodegeneration and cell death. *Autophagy*. 2007;3(6):663–666.
55. Itakura E, Kishi-Itakura C, Koyama-Honda I, Mizushima N. Structures containing Atg9A and the ULK1 complex independently target depolarized mitochondria at initial stages of Parkin-mediated mitophagy. *J Cell Sci*. 2012; 125(pt 6):1488–1499.
56. Hohensinner PJ, Goronzy JJ, Weyand CM. Telomere dysfunction, autoimmunity and aging. *Aging Dis*. 2011;2(6):524–537.
57. Valmori D, et al. Circulating tumor-reactive CD8(+) T cells in melanoma patients contain a CD45RA(+)CCR7(–) effector subset exerting ex vivo tumor-specific cytolytic activity. *Cancer Res*. 2002;62(6):1743–1750.
58. van Lier RA, ten Berge IJ, Gamadia LE. Human CD8(+) T-cell differentiation in response to viruses. *Nat Rev Immunol*. 2003;3(12):931–939.
59. Roederer M, Nozzi JL, Nason MX. SPICE: Exploration and analysis of post-cytometric complex multivariate datasets. *Cytometry A*. 2011;79(2):167–174.
60. Young AR, et al. Starvation and ULK1-dependent cycling of mammalian Atg9 between the TGN and endosomes. *J Cell Sci*. 2006;119(pt 18):3888–3900.